FINAL PHASE 1 REPORT DE-EE0007698: A NOVEL APPROACH TO MAP PERMEABILITY USING PASSIVE SEISMIC EMISSION TOMOGRAPHY

Ian Warren

Ormat Technologies Inc.

Erika Gasperikova

Lawrence Berkeley National Laboratory

Satish Pullammanappallil

SubTerraSeis, LLC

EXECUTIVE SUMMARY

The utility of passive seismic emission tomography for mapping geothermal permeability has been tested at two locations in northern Nevada, San Emidio and Crescent Valley. The San Emidio study area overlaps a geothermal field in production since 1987 and also a new, hotter resource recently drilled to the south of the production field. In contrast, the subsurface at the Crescent Valley study area is poorly constrained by drilling with geothermal potential mainly indicated by geothermometry of hot spring discharges, shallow, high heat flow, and reports of blown out mineral exploration wells.

Newly acquired magnetotelluric data and passive seismic data collected with tightly spaced geophone arrays are combined with historic drilling, active seismic, and potential fields data to generate 3-D permeability maps. A cooperative inversion methodology has been developed using active seismic, magnetotelluric, and gravity data in order to produce more robust velocity models for passive seismic data processing without requiring expensive 3-D active seismic surveys. The cooperative inversion estimates velocities from other geophysical data where no prior seismic velocity information is available.

At San Emidio, permeability associated with the known geothermal reservoir coincides with acoustic energy anomalies defined by passive seismic emission tomography and with low resistivity anomalies defined by magnetotelluric data while the structural setting of these anomalies is constrained by drilling, gravity, and other geophysics, and refined with cooperative inversion results. At Crescent Valley, acoustic energy anomalies defined by passive seismic emission tomography and low resistivity anomalies defined by magnetotelluric data occur down-

dip from and basin-ward of hot springs discharging along the main range-front fault. These anomalies are located where range-front-parallel faulting potentially intersects faulting associated with a NNW-trending horst that is defined by geophysics and drilling, including historic mineral well blow outs. With limited subsurface data, cooperative inversion maximizes the utility of magnetotelluric data at Crescent Valley by using them to estimate seismic velocities that refine processing of passive seismic data and to refine resistivity patterns to better define structures controlling geothermal permeability.

A robust 3-D permeability map can be created using magnetotelluric and dense passive seismic datasets when they are combined with drilling and potential fields datasets that help constrain the structural and geological controls on geothermal permeability. Cooperative inversion of seismic and magnetotelluric datasets provides more robust and location-specific velocity models that optimize processing and interpretation of passive seismic data while also increasing the utility of magnetotelluric data for identifying structures that control geothermal permeability.

Using the methodologies developed herein, proposed drill targets have been selected at San Emidio and Crescent Valley for testing during Phase 2.

1. Introduction

Geophysical methods have been applied to exploration and development of geothermal resources for decades, and geophysical techniques have continued to advance in terms of resolution and robustness of inversion constraints, particularly owing to ever greater computational capabilities. Despite this, no technique has been developed to consistently and robustly map subsurface permeability of geothermal resources. Integrated drilling, geology, and geophysics datasets are the current state-of-the-art for creating 3-D permeability maps; however, only drill intersections of reservoirs precisely locate permeability and other datasets do so by proxy with varying degrees of success.

Passive seismic emission tomography (PSET) techniques are used by the oil and gas industry to map fracture-controlled permeability in unconventional reservoirs, and magnetotelluric (MT) techniques are used in the geothermal industry to map hydrothermal alteration and conductive brine. Velocity models are required for passive seismic data processing; however, these are typically developed from expensive, high impact, active seismic surveys. Preliminary processing using simple, layer-cake velocity models gave encouraging results (Warren et al., 2018); however, more robust velocity models are important for maximizing the utility of passive seismic data. A cooperative inversion strategy using active 2-D seismic and MT datasets from San Emidio was developed to enable generation of robust 3-D velocity models for final processing of the passive seismic datasets. Additionally, the cooperative inversion potentially can estimate 3-D velocity structure from available MT and gravity data. Project tasks, planned and actual schedules, and progress/completion are summarized in Table 1. Table 2 summarizes Phase 1 expenses with only a minimal amount of report preparation time in Q1 2019 not included.

Major Task Schedule									
Phase	SOPO Task #	Item: Task = T Milestone = M Deliverable = D	Task Title or Milestone/Deliverable Description	Original Planned Start Date	Actual Start Date	Original Planned Completion Date	Actual Completion Date	% Complete	Progress Notes
1	1	T	Project Management and Planning	9/1/2016	10/1/2016	ongoing	ongoing	98%	ongoing
1	2	T	Historic Data Review and Organization	9/1/2016	10/1/2016	10/31/2016	in progress	100%	completed
1	3.1	T	Passive seismic survey design	9/1/2016	10/1/2016	10/31/2016	11/8/2016	100%	completed
1	3.1	M	Design and confirm the final passive seismic surveys	9/1/2016	10/15/2016	10/31/2016	11/8/2016	100%	completed
1	3.2	T	Passive seismic survey scheduling	10/31/2016	10/31/2016	12/31/2016	12/18/2016	100%	completed
1	3.2	M	Passive seismic data collection scheduled and completed at both sites	10/31/2016	12/1/2016	12/31/2016	12/18/2016	100%	completed
1	3.3	T	Passive seismic survey processing and evaluation	11/1/2016	1/1/2017	4/30/2017	4/30/2017	100%	completed
1	3.3	M	Passive seismic datasets finalized	11/1/2016	1/10/2017	4/30/2017	4/30/2017	100%	completed
1	4.1	T	San Emidio EM survey design	9/1/2016	10/1/2016	10/31/2016	10/28/2016	100%	completed
1	4.1	M	Final San Emidio survey design confirmed with contractor	9/1/2016	10/30/2016	10/31/2016	10/28/2016	100%	completed
1	4.2	T	San Emidio EM survey scheduling	10/31/2016	10/28/2016	11/30/2016	9/15/2017	100%	completed
1	4.2	M	San Emidio EM survey scheduled and contract completed with Quantec	10/31/2016	10/30/2016	10/31/2016	10/28/2016	100%	completed
1	4.3	T	San Emidio EM data evaluation	11/1/2016	11/1/2016	12/31/2016	12/4/2017	100%	completed
1	4.3	M	Final 3-D resistivity model completed for San Emidio	12/4/2017	12/4/2017	12/31/2016	12/4/2017	100%	completed
1	4.4	T	Crescent Valley EM survey design	11/1/2016	3/1/2017	2/28/2017	6/30/2017	100%	completed
1	4.4	M	Final Crescent Valley EM survey design	2/1/2017	3/1/2017	2/28/2017	6/30/2017	100%	completed
1	4.5	T	Crescent Valley EM survey scheduling	2/1/2017	6/30/2017	5/31/2017	9/30/2017	100%	completed
1	4.5	M	Crescent Valley EM survey scheduled and contract completed with Quantec	2/1/2017	6/30/2017	5/31/2017	9/30/2017	100%	completed
1	4.6	T	Crescent Valley EM data evaluation	6/1/2017	10/1/2017	7/30/2017	10/31/2017	100%	completed
1	4.6	M	Final 3-D resistivity model completed for Crescent Valley	6/1/2017	10/1/2017	7/30/2017	4/30/2018	100%	completed
1	5.1	T	Seismic-EM cooperative inversion development	12/1/2016	1/1/2018	8/31/2017	5/31/2018	100%	completed
1	5.2	T	Seismic-EM cooperative inversion	7/1/2017	3/15/2018	9/30/2017	5/31/2018	100%	completed
1	6.0	M	Final velocity models	8/1/2017	4/30/2018	9/30/2017	6/19/2018	100%	completed
1	7.0	M	Final semblance volumes	9/1/2017	6/22/2018	11/30/2017	11/30/2018	100%	completed
1	8.0	M	Final 3-D permeability maps	10/1/2017	12/1/2018	2/28/2018	1/28/2019	100%	completed
1	8.1	T	Final permeability map assessment	10/1/2017	1/7/2019	12/31/2017	1/28/2019	100%	completed
1	8.2	T	Data integration and well targeting	12/1/2017	12/1/2018	2/28/2018	1/28/2019	100%	completed
1	8.3	T	Final well siting	2/1/2018	1/21/2018	2/28/2018	1/28/2019	95%	TBD

Table 1. Project tasks, milestones, and schedule

Spending Summary for SF 424A Budget Forms				
Object Class Categories	Approved Budget	Project Expenditures		% Spent to date
Per SF 424a		This Quarter	Cumulative to Date	
a. Personnel	$15,042	$5,952	$70,623	470%
b. Fringe Benefits				
c. Travel	$5,100		$2,133	42%
d. Equipment				
e. Supplies				
f. Contractual	$1,223,752	$10,000	$1,080,575	88%
g. Construction				
h. Other				
i. Total Direct Charges (sum of a to h)	$1,243,894	$15,952	$1,153,331	93%
j. Indirect Charges				
k. Totals (sum of i and j)	**$1,243,894**	**$15,952**	**$1,153,331**	93%
DOE Share	$976,612	$10,000	$880,200	
Cost Share	$267,283	$5,952	$273,132	
Calculated Cost Share Percentage	21.5%	37.3%	23.7%	
*budget justification documents updated in November 2017 to reflect all passive seismic contracting expenses being in Phase 1				

Table 2. Summary of project expenses.

Figure 1: Project Locations. San Emidio power plant and vicinity, Washoe Co., NV and Crescent Valley, Eureka Co., NV.

2. Study Areas

Study areas are located at San Emidio and Crescent Valley, Nevada (Figure 1). At San Emidio, geothermal power has been produced since 1987. Abundant production, drilling, geologic, and geophysical data mean that the subsurface is well constrained. Additionally, recent drilling at San Emidio has identified new, higher temperature resource south of the currently producing field. In contrast, much less is known about the subsurface at Crescent Valley where project activities are focused in the area of hot spring discharges along the Crescent Valley fault with chalcedony geothermometry indicating a ~160˚C reservoir at depth. The two locations allow testing of permeability mapping techniques at a well constrained "training" site and also at a "greenfield" exploration site. At both sites, new data collections occurred in the vicinity of step-overs in range front faults, sites favorable for development of geothermal systems (Faulds et al., 2011). Additionally, Crescent Valley was deemed one of the most prospective areas for discovering a geothermal resource based on results of University of Nevada Reno's Play Fairway analysis project (Faulds et al., 2016).

2.1 San Emidio Geologic and Geothermal Setting

The San Emidio Desert is located within the actively extending northwestern Basin and Range of Nevada, approximately 100 km north of Reno. San Emidio lies within a transtensional tectonic setting between northwest-directed shear to the west associated with the Walker Lane and west-

northwest to east-west extension to the east associated with the western Basin and Range (Bennett et al., 2003; Hammond and Thatcher, 2005; Hammond et al., 2009).

The geology of the San Emidio area is known from exposures in the northern Lake Range and from drilling associated with geothermal exploration and development in the basin to the west that lies in the hanging wall of the Lake Range fault. Mesozoic metamorphic rocks are overlain by Tertiary volcanic and sedimentary rocks that host the geothermal reservoir. Variable hydrothermal alteration is associated with the active geothermal system and occurs along the San Emidio Fault north to the Wind Mountain Mine (Bonham and Papke, 1969; Drakos, 2007, Rhodes et al., 2010, 2011; Figure 2).

The San Emidio Geothermal Area first produced power in 1987 with a 3.6 MW binary plant fed by shallow, 148˚C wells. After U.S. Geothermal Inc. acquired the project in 2008, work began to maximize the production potential, and a new 14.7 MW plant was commissioned in 2012. Ormat is the current owner after completing acquisition of U.S. Geothermal Inc. in April 2018. Over the life of the project, production has ranged from <3000 gpm to >4500 gpm at temperatures of 140-148˚C. From 2015 to 2017, drilling south of the producing field discovered a new, hotter (>160˚C) resource that is currently in the early development stages.

San Emidio wells produce primarily from depths of ~1700 to 2300 feet (~520-700 m) below surface from fractures hosted by silicified tuff and intermediate to mafic composition lavas. The top of the reservoir generally follows the contact between overlying, mechanically weak, commonly clay-altered volcaniclastic rocks and underlying, mechanically strong, silicified tuff and lavas. The shallow injection zone is associated with massive silicification of tuff and tuffaceous sedimentary rocks; it is poorly connected to production wells, and most injectate flows north in the shallow subsurface. The newly discovered resource to the south has a similar geologic setting with the reservoir hosted by fractured, silicified tuff and lava which are overlain by clay-altered, volcaniclastic rocks.

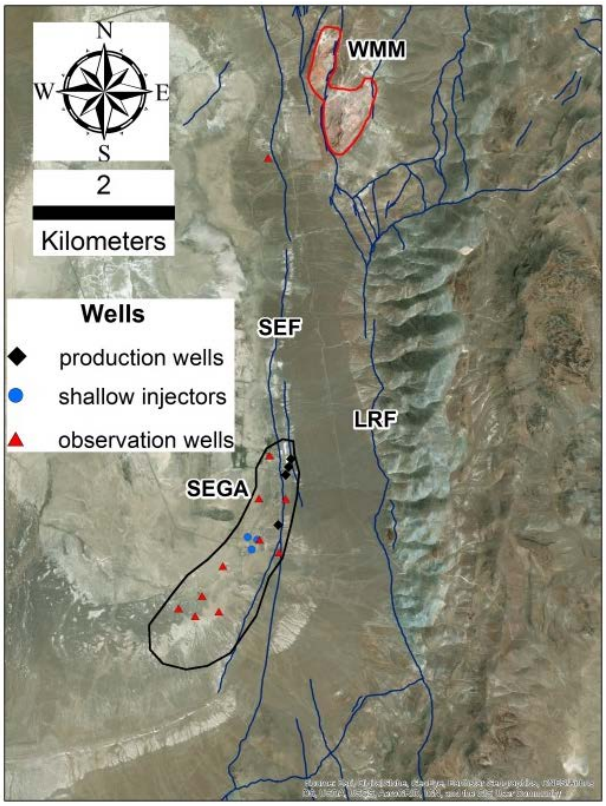

Figure 2: Southeastern San Emidio Desert and the San Emidio Geothermal Area (SEGA), Washoe County, NV. LRF-Lake Range fault; SEF-San Emidio fault; WMM-Wind Mountain Mine. Active and monitor wells show the extent of the currently defined resource area which is open to the south and west. Bleached and Fe-stained rocks along the SEF and LRF and in the vicinity of the WMM are hydrothermally altered. Green-blue-gray exposures in the footwall of the west-dipping LRF are Mesozoic metamorphic rocks which are overlain by Tertiary rocks that dip to the east. Dark blue faults are from Rhodes et al. (2011).

2.2 San Emidio Geophysics

Ground gravity and magnetic surveys have been completed over the known geothermal resource area, and these surveys were extended to the south and west in 2016. Most notable from these datasets are features within the step-over in the range front fault south of the San Emidio wellfield. A refined structural model of the current study area has been guided by 2-D modeling of gravity data (Figure 3).

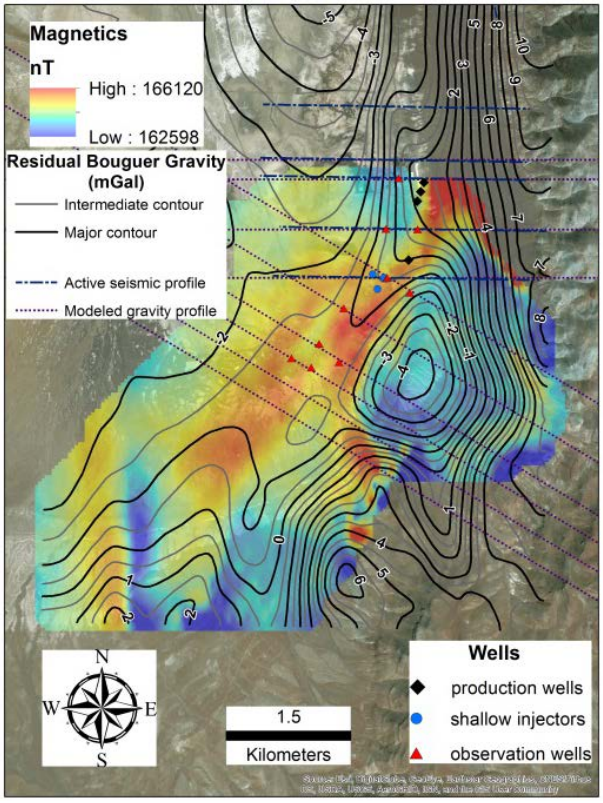

Figure 3: San Emidio ground gravity and magnetics. Magnetics symbolized with warm to cool colors (high to low nanotesla values) are overlain by residual Bouguer gravity contours (mgal) to show the complex structural setting of the range-front step-over. Also shown are locations of modeled gravity profiles and historic 2-D seismic lines.

From 2010 to 2014, DOE-funded innovative exploration research completed nine active seismic profiles (five southernmost shown in Figure 3), detailed structural and slip tendency analyses, PSInSAR ground deformation studies (Eneva et al., 2011), and drilling and deepening of eight observation wells to test these methods (Teplow and Warren, 2015). The active seismic profiles imaged the main range-front fault, but resolution of other structures, particularly in volcanic +/- hydrothermally altered rocks, was generally poor. Velocity modeling of the seismic profiles showed complex patterns of velocity gradient related to structure and possibly hydrothermal alteration (Figure 4). Slip tendency analyses confirmed north- to north-northeast-trending faults as most likely to dilate in the current regional stress regime. PSInSAR highlighted probable structural boundaries to subsiding areas associated with production wells, and tumescent areas associated with shallow injection. Drilling intersected highest temperatures drilled in the field (162˚C) adjacent to and below the main production zone, and expanded the known permeable reservoir to the south (Figures 2 and 3; southernmost production well).

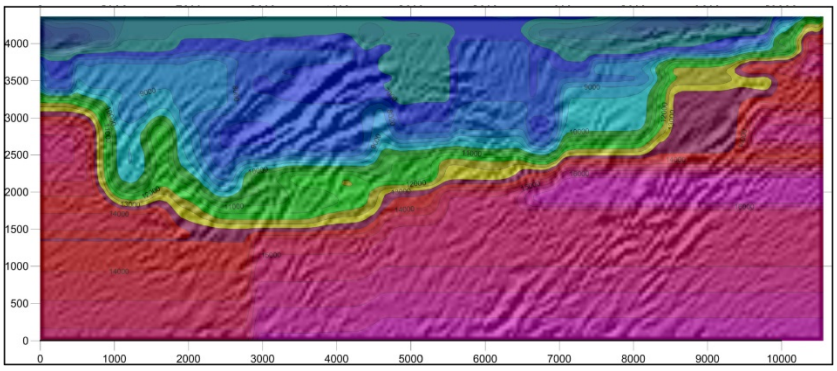

Figure 4: San Emidio Seismic Line 9 (southernmost, Figure 3). P-wave velocity model overlain on migrated seismic reflection profile shows structural complexity across the geothermal reservoir.

2.3 Crescent Valley Geologic and Geothermal Setting

The Crescent Valley project area is located in Eureka County, NV. It is bounded to the east by the Cortez Range and to the northwest by the Dry Hills; surface geothermal manifestations occur along the Crescent Valley and Dry Hills faults. The valley between the southern end of the Dry Hills and the Cortez Range was previously drilled by mineral explorers who lost control of core holes when they intersected artesian, flashing fluid at depths of ~2000 feet (~600 m) below surface. Geothermometry of hot spring discharges suggests reservoir temperatures at depth in excess of ~160˚C.

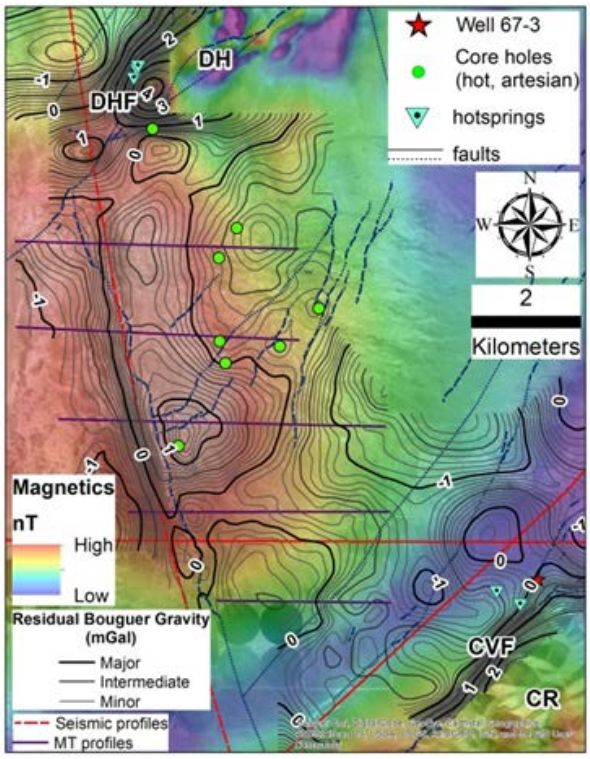

Figure 5: Crescent Valley geothermal project, Eureka Co., NV. CR-Cortez Range; CVF-Crescent Valley fault; DH-Dry Hills; DHF-Dry Hills fault. This study is focused in the area where hot springs discharge from

the CVF. Mapped faults are from McConville et al. (2017). Residual Bouguer gravity contours are overlain on total magnetic intensity.

Crescent Valley is a basin primarily filled with Tertiary-Quaternary sedimentary rocks. The southern end of the Dry Hills, known as Hot Springs Point, comprises Tertiary volcanic rocks, Jurassic granodiorite, and Paleozoic metasedimentary rocks that make up the footwall of a northwest-dipping range-front fault (DHF) along which discharge chloride-bicarbonate springs. In the Cortez Range, Jurassic granodiorite makes up the footwall of the northwest-dipping Crescent Valley fault (CVF) along with minor occurrences of Tertiary volcanic rocks and dikes. Fluids discharged from hot springs along the CVF are distinct from those at Hot Springs Point with notably less bicarbonate, and they are near-boiling with silica geothermometry indicating reservoir temperatures >160˚C. Mineral exploration core holes, gravity, and 1980s active seismic profiles identified an uplifted horst that stretches across the valley, trending north-northwest from the Crescent Valley fault south of the aforementioned hot springs to Hot Springs Point. The horst is made up of Paleozoic carbonate and siliciclastic rocks intruded by Jurassic granodiorite, and overlain by Tertiary mafic lava and Tertiary-Quaternary sedimentary rocks. At Hot Springs Point and in the vicinity of hot springs along the CVF, epithermal precious metals mineralization and associated hydrothermal alteration are present and have been explored by multiple companies.

Crescent Valley was explored in the late 1970s by Chevron who completed 31 shallow temperature gradient wells that defined several square kilometers of anomalous heat flow. Core holes in the middle of the valley and adjacent to the horst were drilled in the 2000s by Montezuma Mines (Figure 5). Some of these encountered artesian, flashing fluid, but no fluid samples were collected and no equilibrated downhole temperatures were measured. In late 2015 and early 2016, U.S. Geothermal drilled well 67-3. A relatively shallow intersection of the range-front fault showed modest permeability and temperature; temperature surveys suggest downhole flow of cool water and chemistry indicates dilution relative to hot spring samples. Ormat is the current owner after completing acquisition of U.S. Geothermal in April 2018.

2.4 Crescent Valley Geophysics

A number of geophysical surveys have been completed at Crescent Valley related to hydrocarbon and minerals exploration. These include four active seismic profiles, ground gravity, gravity gradiometry, ground magnetics, aeromagnetics, and 2-D electromagnetic profiles (Figure 5). A densely spaced ground gravity survey in the vicinity of hot springs along the CVF was completed in 2015. Since then additional work has been done in the area including additional gravity data collection, seismic reinterpretation, structural mapping, and fluid sampling associated with the University of Nevada Reno's DOE-funded, Play Fairway project (McConville et al., 2017).

This study is focused in the vicinity of the hot springs discharging along the CVF. Preliminary structural modeling has been guided by surface measurements along the trace of the CVF, orientation of veins, breccia, and hydrothermal alteration along and adjacent to the CVF, 2-D modeling of gravity, and interpretation of an east-west oriented, historic 2-D seismic profile.

3. SubTER Project Data Collections

Passive seismic data collections were completed at San Emidio and Crescent Valley in late 2016 by Microseismic Inc (Figure 6). At San Emidio, 1302 stations with 6 wired geophones connected to OYO GXR recorders together collected data for nearly 180 hours. At Crescent Valley the same equipment deployed at 989 stations together collected data for 75 hours. Surveys were designed to focus on an area of the subsurface approximately 1700 m x 2200 m x 300 m and initial processing focused on depths of ~600 m to 900 m below surface. Preliminary processing employed a simple, layer-cake, velocity model that was guided by the velocity structure of seismic line 9 at San Emidio, and it was modified to create best matches to downhole string shots in wells near the center of the passive seismic arrays. Final results were processed using robust velocity models produced using a seismic-MT cooperative inversion strategy (described in Section 4). Several large discrete events were also used to calibrate the San Emidio velocity model. Residual static solutions applied across the entire datasets were applied to bring all the traces used in the beamformer into phase. The average absolute positional error of the string shots used to verify this calibration is 1m in the X and Y directions and 3m in the Z direction. For San Emidio a list of discrete microseismic events and a 1680m x 2190m x 600m PSET volume of acoustic energy were delivered. For Crescent Valley no discrete events were identified, and a 1750m x 2250m x 300m PSET volume of acoustic energy was delivered.

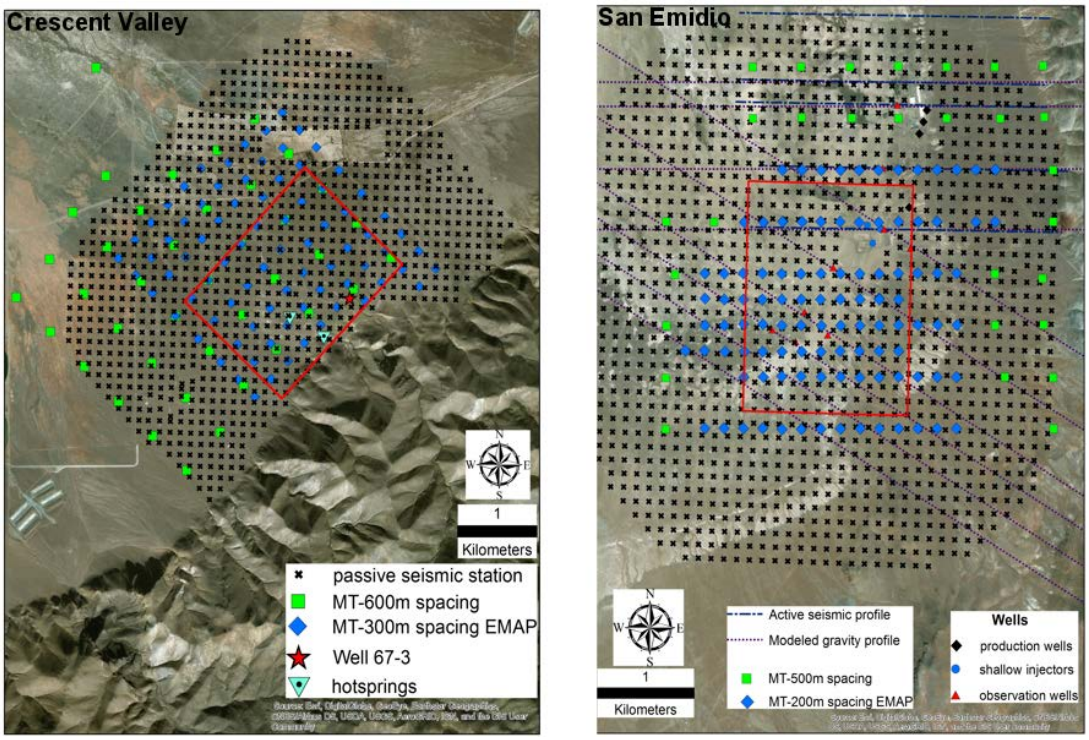

Figure 6: Passive seismic and electromagnetic data collections at Crescent Valley (left) and San Emidio (right). Red boxes show the ~1700m x 2200m x 300m focus area.

MT data collection at San Emidio started in late 2016; due to low natural signals the results were not satisfactory, and measurements over a portion of the survey area were repeated and completed over two field campaigns in summer 2017. Data collection at Crescent Valley was completed in September 2017. The MT data acquisition (250 Hz-0.001 Hz) at both locations was done by Quantec Geoscience USA Inc (Figure 6). In addition to these two surveys, at Crescent

Valley, Quantec also acquired Audio-MT (AMT) (10 kHz – 0.001 Hz) data along 10 profiles, and provided 2-D inversions and interpretation of these data. The interpretation of AMT data was aimed at identifying faults and shallow structures in the study area.

3.1 Passive Seismic Processing

The passive seismic data collected at the San Emidio site were processed using two closely related passive seismic imaging techniques based on beamforming of the high-frequency approximation of the wave equation. The first technique applied to the data is aimed at identifying discrete events with an impulsive character (Duncan and Eisner, 2010) using the Microseismic Inc. (MSI) Passive Seismic Emission Tomography algorithm using a time window for imaging of 50 milliseconds. In order to estimate the hypocenter location and origin time of a microseismic event, the array is beamformed onto a series of points in the subsurface. Beamforming is accomplished using travel-time correction and stack response. The stack is performed across all recorded traces for the entire length of the recording interval and for each cell in the processing volume, and each beamformed trace is an estimate of the acoustic history of the focus point. Once the family of related responses for an event is isolated, a maximum likelihood estimator is used to finalize the event location and origin time. The direction of first motion and the observed amplitude across the array were used to derive focal mechanisms for several large, discrete events at San Emidio, while no discrete events other than the downhole string shot were identified at Crescent Valley.

The second technique, Ambient Passive Seismic Imaging, is a close analog to the more conventional approach described above and accomplished using MSI's repetitive Passive Seismic Emission Tomography using a time window for imaging of 1 hour. The principal difference is that it relies on longer duration stacking within the beamformer to suppress random noise and allow for smaller ambient or repetitive signals to image. The increased duration of the stacking window sacrifices precise source time for increased noise suppression; therefore, it is not possible to estimate a discrete hypocenter or event origin time from a formed beam. The technique provides a holistic view of acoustic history using the long duration aggregation of multiple formed beams (Jeremic at al., 2016). Figure 7 schematically illustrates the difference between the processing methods. Throughout this report, we use PSET to refer to MSI's repetitive passive seismic emission tomography, in contrast to discrete events identification with the passive emission tomography algorithm.

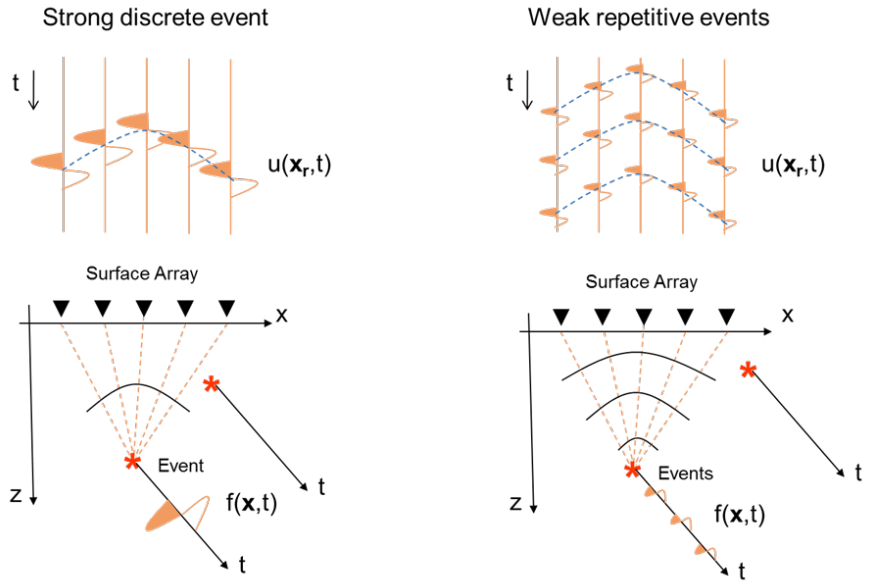

Figure 7. Schematic illustration of the variation between Microseismic Inc.'s processing techniques.

3.2 Magnetotelluric data processing and inversion

MT data were processed using the traditional remote reference approach with remote sites located 30-60 miles away from the survey area. The data were also processed using multi-station robust processing (Egbert, 1997) with at least four stations acquired simultaneously.

MT data at San Emidio were collected with the configurations shown in Figure 8. Each standalone sounding site was configured with L-shaped magnetic sensors and 200 m long E-field dipoles (Ex, Ey) (Figure 8, left); sites along profile lines used double (mirrored) L configurations (Figure 8, right). This configuration, with continuous sampling of the E-field along the profile, is called an electromagnetic array profiling (EMAP). The survey area was ~5x5 km, and 2D MT inversion was done along 10 profiles running east-west. The resistivity structures recovered by 2D inversion were then stitched into a 3D resistivity cube by interpolating between the profile lines.

MT data at Crescent Valley were collected with the standalone sounding site configuration (Figure 8) over a survey area of ~6x4 km. 2D MT inversions were done along profiles running perpendicular to the range-front fault (CVF). The results were then stitched into a 3D resistivity cube by interpolating between the profile lines.

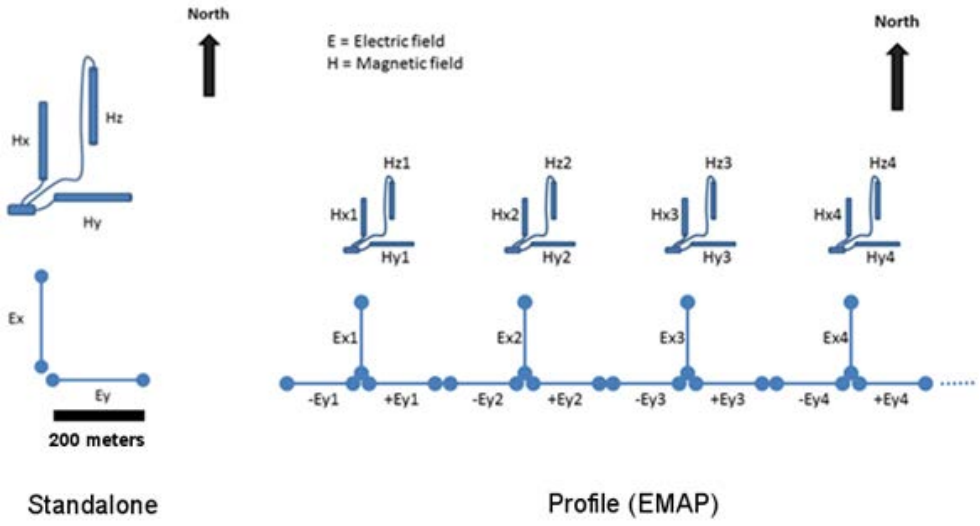

Figure 8: MT sounding site configurations

4. Seismic-MT Cooperative Inversion

The potential for development of a useful seismic-MT cooperative inversion is predicated on the relationship between resistivity and velocity via porosity (Faust, 1953; Hacikoylu, et al., 1996; Ursin and Carcione, 2007; Werthmuller, et al., 2013). The approach for this study was to bypass the need for multiple regressions and computation of porosity through the use of a supervised learning technique that related resistivity to velocity directly through a neural network regression.

When multiple observations of different types are made for a subsurface region, each observation type and its derived products are affected by the same physical characteristics of the region. While each observation may be affected differently, the observations when expressed as a parameterized model, may establish regions of similarity in a "fuzzy" (Zadeh, 1965) sense. These regions of similarity can be exploited to refine the observations. The strategy deployed for this study is to identify these regions of similarity through fuzzy pattern recognition techniques and to cooperatively refine the observation set using the results from the pattern recognition.

The pattern recognition approach is based on fuzzy c-means clustering (Dunn, 1973, Bezdek et al., 1984). The fuzzy clustering approach partitions the input space into a predetermined number of clusters. A measure of how well an input point "fits" into each cluster is also determined. The clustering process is a non-linear optimization problem that is solved by iteratively minimizing an objective function.

Development of the cooperative inversion was executed in two phases. Phase 1 focused on the well-studied and data-rich San Emidio area. Data acquired along 2-D seismic profiles at San Emidio were used to jointly refine the input seismic velocities by exploiting the physical similarities between the variables while adding detail and identifying outliers. Specifically, long-wavelength features of resistivity were used to constrain the deeper horizons of the two-dimensional velocity model. In addition, the modeled density contrast between basin fill and basement was used to constrain this important resistivity and velocity boundary. These results were then used in a neural network estimation process to extend the seismic velocities to cover

the region defined by the 3-D resistivity volume. In Phase 2, the trained model from Phase 1 was used to estimate P-wave velocities for Crescent Valley, a greenfield exploration site with no prior detailed velocity information and minimal subsurface data.

All observations were resolved to a common data set based on the seismic lines from the active source seismic imaging at San Emidio. The observations were then normalized on the unit interval [0,1] using a min-max normalization and a parametric model was constructed comprised of four-dimensional points (4-D) on the 4-D unit hyper-cube. The input variables at San Emidio include: resistivity derived from inversion of magnetotelluric observations, P-wave and S-wave velocities derived from active source seismic imaging along 2-D linear profiles, and density contrast derived from modeling of gravity data. The input variables and final velocity models were constructed with resolution of 50m x 50m x 10m.

The refinement process involved cluster analysis (Figure 9). It began with a data exploration phase where the refinement parameters, including clustering method, fuzziness, and the number of clusters were optimized. Clustering methods evaluated include Fuzzy C-Means (Dunn, 1973; Bezdek et al., 1984), Gustafson-Kessel (Gustafson and Kessel, 2000) and Gath-Geva (Gath and Geva, 1989). For validation of clustering results, Xie-Beni (Xie and Beni, 1991), Partition Coefficient (Bezdek, 1973), and Partition Entropy (Bezdek, 1974) cluster validation indexes where utilized. No single validation index was sufficient for validation, and all were considered when evaluating cluster results. Cluster sizes of 6, 10, 20, 30, 40, 80, and 100 were evaluated, each with multiple fuzziness values, and it was determined that the improvement using cluster sizes above 40 and fuzziness equal 2.0 was not significant.

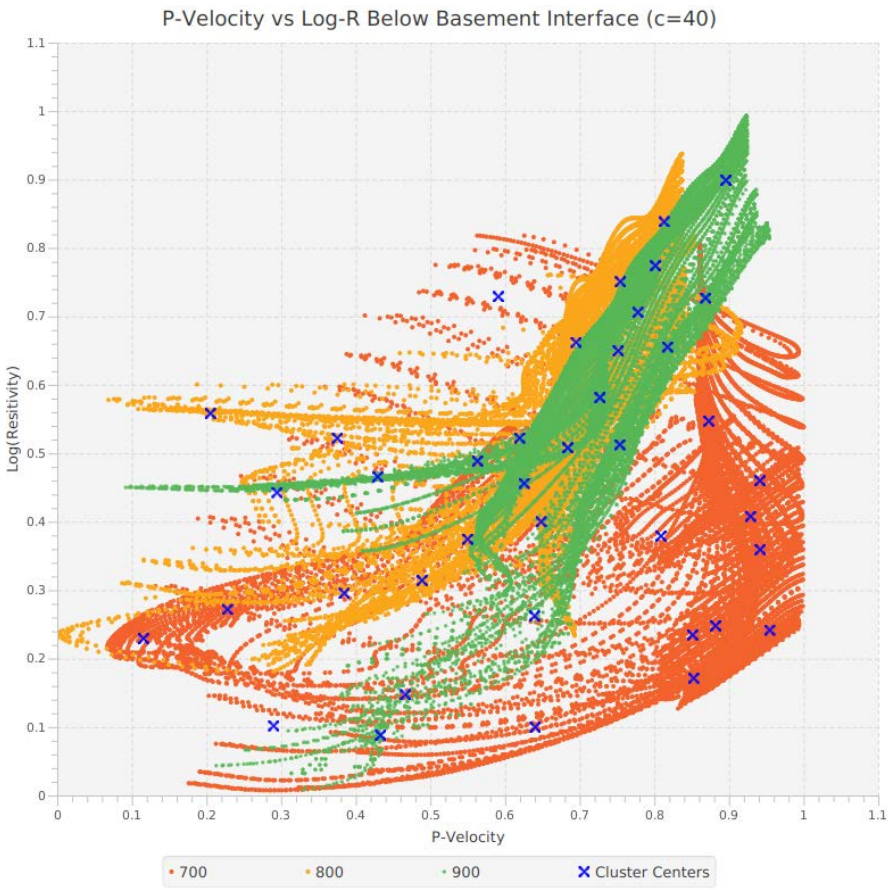

Figure 9. Graphical representation of cluster analysis

In order to extend P-wave and S-wave velocities throughout the resistivity and density contrast volumes, a neural network was trained using resistivity-only, density-contrast-only, and resistivity and density contrast inputs which had been interpolated to seismic profile locations. The refined P-wave and S-wave velocities along the 2-D profiles were used as target ideals for the training, and the trained network was then evaluated over the entire 3-D volume.

Based on similar geologic and geothermal settings, and assumption of a similar relationship between P-wave velocity and resistivity at San Emidio and Crescent Valley, the trained network was applied to resistivity and density contrast data at Crescent Valley. Robust results were obtained when the training was done using depth and resistivity, which produced a good match to the modeled basin-basement contact and known structure.

5. Summary of Results

In combination with drilling, geology, and other geophysics datasets, PSET volumes and resistivity volumes are used to map geothermal permeability in the subsurface. At San Emidio, the known geothermal reservoir lets us rigorously compare the data volumes to geothermal permeability. At Crescent Valley, the subsurface is much less constrained; however, the range-front fault system and hot springs provide information about where reservoir fluids discharge to surface and possible

paths between the surface and a geothermal reservoir at depth. Drilling, geology, gravity and magnetics inform the structural models that provide the frame work for evaluating the PSET and resistivity volumes, especially interpretation of faults and stratigraphy from 2-D gravity modeling.

5.1 San Emidio PSET and Resistivity

Figure 10 shows PSET acoustic energy as summed Z-scores for each XY location, creating a 2-D representation of PSET results. The southernmost production well 61-21 is located just beyond the northeastern most corner of the data volume. Fracture permeability associated with the geothermal reservoir continues north from this well and also is intersected by well OW-9 and the northern production wells, 75-16, 75B-16, and 76-16. Modest acoustic energy occurs between the well 61-21 and newly discovered >160°C reservoir intersected by wells 17-21, 18-21, 25-21, 25A-21, and 78-20 except in the vicinity of injection wells 42-21, 43-21, and 53-21. The newly discovered resource is spatially coincident with the largest, contiguous acoustic energy anomaly. Broad areas of anomalous acoustic energy occur to the northwest and are associated with structure expressed in the topography of gravity-modeled basement. The eastern margin of the southern reservoir, as currently understood and defined by high permeability, is marked by wells 45-21 and 28-21 which are hot (>160˚C) but low permeability and with lower shut-in pressure than wells to the west that have intersected the southern reservoir; they sit at the eastern margin of the large acoustic energy anomaly.

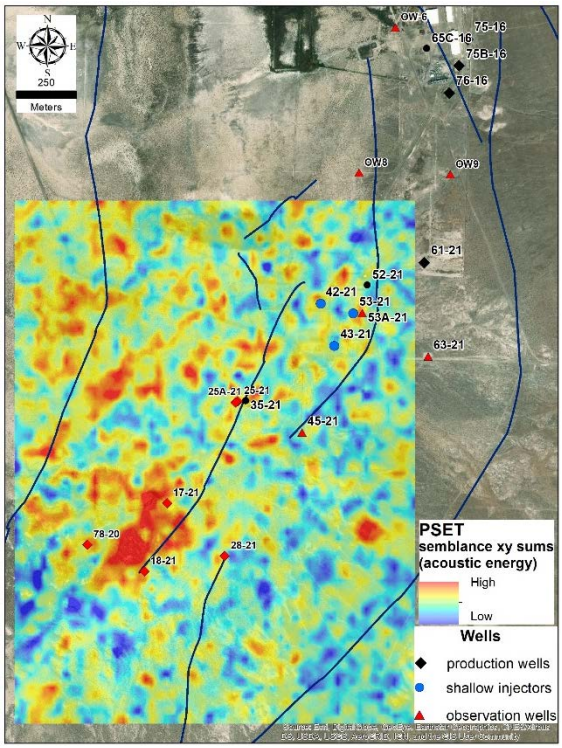

Figure 10: San Emidio PSET volume and modeled faults. PSET volume Z-scores are summed at each XY location to give a 2-D representation of the dataset.

In 3-D, PSET energy can be compared to modeled faults and drilled reservoir intersections. Figure 11 shows PSET energy mapped onto gravity-modeled basement. Faults are expressed in

the topography of the basement and are dominantly north-striking and west-dipping, locally connected by steeply dipping, northeast-striking linkage structures. Relay ramps occur where faults overlap. Simple 2-D gravity modeling using lower density “basin fill” and higher density “basement” effectively demarcates the transition from weak, clay altered volcaniclastic rocks into the underlying, stronger, silicified lava and tuff that host the geothermal reservoir; this boundary is a close proxy for top of the reservoir. Similar to the 2-D representation of Figure 10, high energy characterizes the basement surface west of the low energy eastern boundary of the reservoir. The high energy also occurs along segments of faults through the drilled reservoir and on subparallel faults to the northwest. The high energy areas shown in Figure 11 closely match the current understanding of the southern reservoir based on limited drilling.

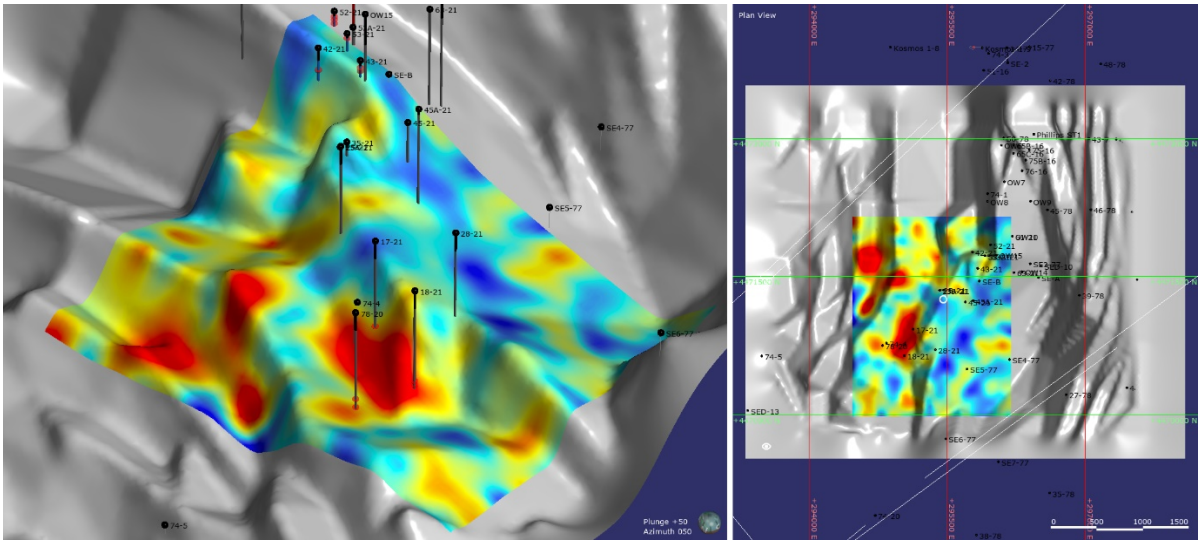

Figure 11: Oblique view looking down and to the northeast of San Emidio PSET volume mapped onto “mechanical” basement (gray), a close proxy to the top of the geothermal reservoir with fault-controlled topography. Colors from cool to warm represent increasing acoustic energy (represented by Z-scores). Wells are shown as black cylinders.

The resistivity profiles at San Emidio show large scale structure associated with the main range-front fault that is similar to velocity modeled along co-spatial seismic lines. The survey area is covered with low resistivity sediments (1-10 Ohm-m) that overlie more resistive volcanic and metamorphic rocks at depth (100-1000 Ohm-m). The range-front fault that bounds the western side of the northern Lake Range is clearly identified by the contrast between the high resistivity footwall and the low resistivity hanging wall, and work is ongoing to investigate finer scale structure. When the preliminary resistivity volume is mapped onto faults and mechanical basement (Figure 12), anomalously low resistivity, potential reflecting hydrothermal alteration and conductive brine associated with the geothermal reservoir maps onto a subtle, faulted ridge into which most drilling has been completed. Though all wells do not intersect highly permeable reservoir, they are all hot and intersect mechanically strong, silicified lava, tuff and metamorphic rock at depth, i.e., reservoir rocks. The resistivity thus far provides a somewhat coarse scale view of structure and potentially maps not only the high permeability reservoir, but also adjacent, lower permeability rocks that provide reservoir storage and are saturated with geothermal brine.

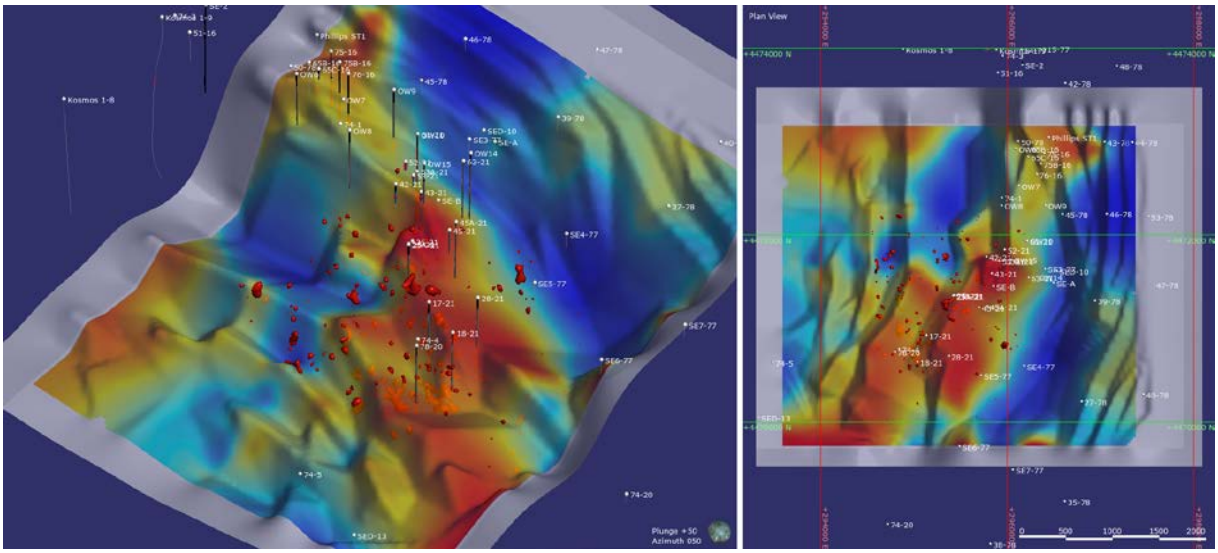

Figure 12: Oblique view looking down and to the northeast of San Emidio resistivity volume mapped onto "mechanical" basement, a close proxy to the top of the geothermal reservoir with fault-controlled topography. Warm to cool colors map low to high resistivity. Wells are shown as black vertical lines. Red volumes are highest 1% PSET values

5.2 Crescent Valley PSET and Resistivity

The subsurface at Crescent Valley is less well known, so interpretation of results is less constrained. Figure 13 shows PSET energy summed at each XY location to give a 2-D representation of the dataset. An anomalous area of high energy occurs basin-ward from the hot springs associated with faults subparallel to the main range front and complex subsidiary fractures related to the right-hand step-over. Using a similar strategy as at San Emdio, data volumes also have been mapped onto faults measured at surface and interpreted from seismic profiles and modeled gravity. Figure 14 shows PSET energy mapped onto faults; anomalous segments of the faults are generally located down dip and basin-ward from the hot springs at the southwest end of the range-front step-over. Similar to San Emidio, low resistivity sedimentary rocks overlie more resistive granodiorite +/- Tertiary volcanic rocks +/- Paleozoic sedimentary rocks. The resistivity structure shows the main range-front fault, as well as two other range-front-parallel faults, and variable basin fill thickness overlying the basement. A slice through the resistivity volume (Figure 16) that runs through the hot springs and is oriented perpendicular to the range-front fault shows a conductive anomaly that is cospatial with geothermal upflow to the the range front and outflow into the basin, consistent with heat flow anomalies defined by 1970s temperature gradient drilling.

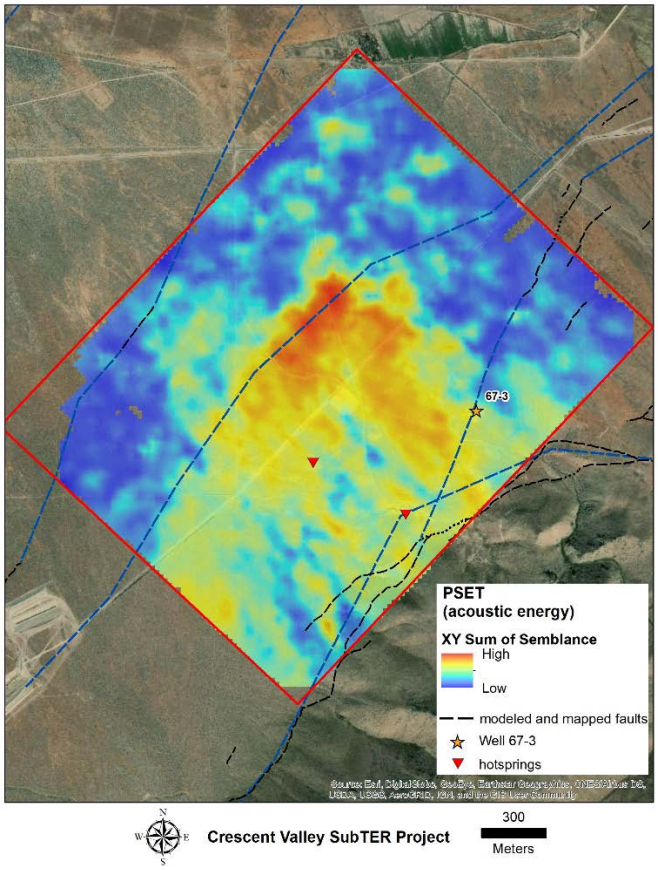

Figure 13: Crescent Valley PSET volume Z-scores are summed at each XY locations to give a 2-D representation of the dataset. Orange star is well 67-3. Red inverted triangles are hot springs. Dark blue faults are from McConville et al. (2017) and from geological and gravity modeling.

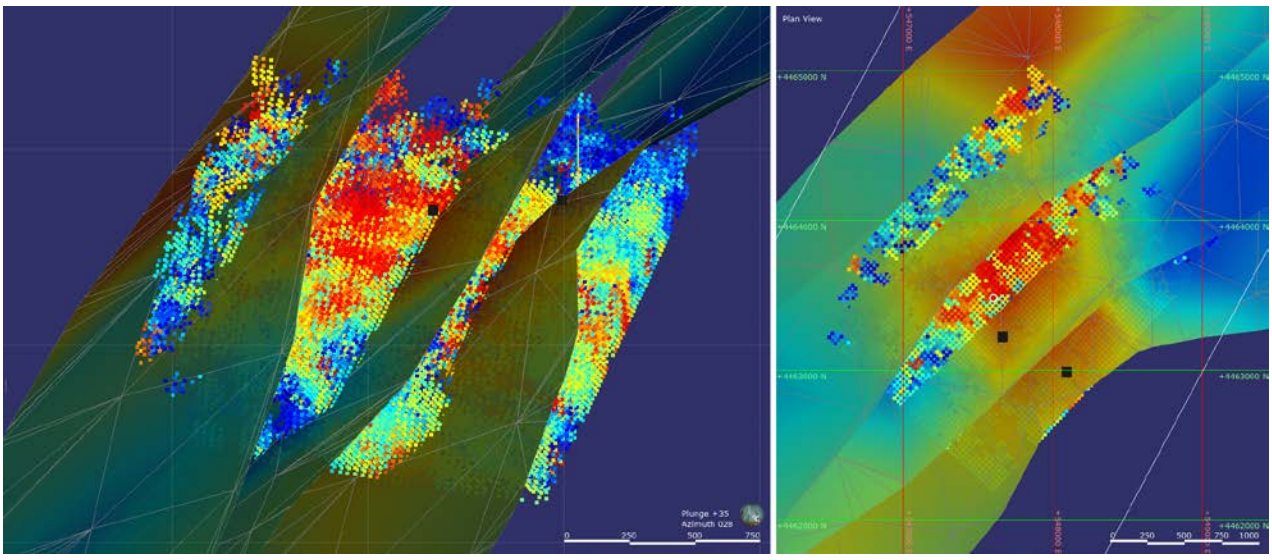

Figure 14: Oblique view looking down and to the north-northeast of Crescent Valley PSET volume mapped onto faults with cool to warm colors representing low to high energy. Modeled faults dip to the northwest.

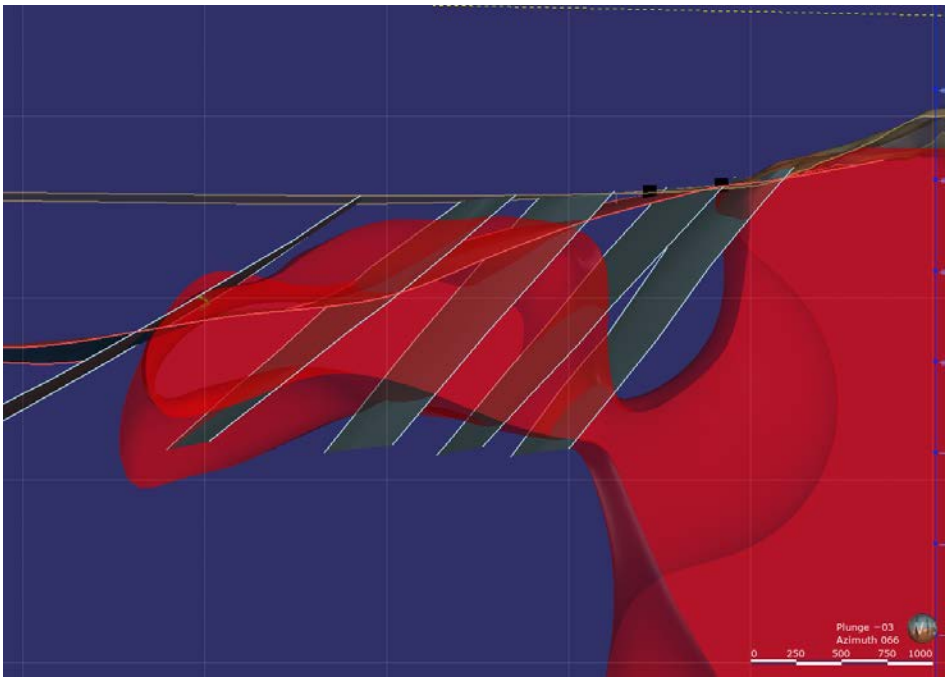

Figure 15. Low resistivity volume related to main range front and subparallel faults that downstep into the basin. Black squares are hot springs. Topographic surface is tan; gravity-modeled top of basement is pink.

5.3 Seismic-MT Cooperative Inversion Results

Seismic velocity volumes were created using cluster analysis of velocity, resistivity, density contrast, and depth along active seismic profiles at San Emidio to refine datasets. The refined datasets were used to train neural networks in order to estimate seismic velocities throughout the region of the San Emidio and Crescent Valley resistivity volumes.

The cluster-analysis-refined datasets at San Emidio show good correlation to patterns of original datasets, geology, and structure (Figures 16, 17, 18). The Crescent Valley data volumes generated using the San-Emidio-trained neural network are validated with similar patterns preserved in the modeled resistivity as in the MT-derived resistivity. These validation results suggest that a robust velocity model can be generated using the cooperative inversion methodology that employs cluster analysis and training of a neural network to estimate seismic velocity from MT and gravity datasets.

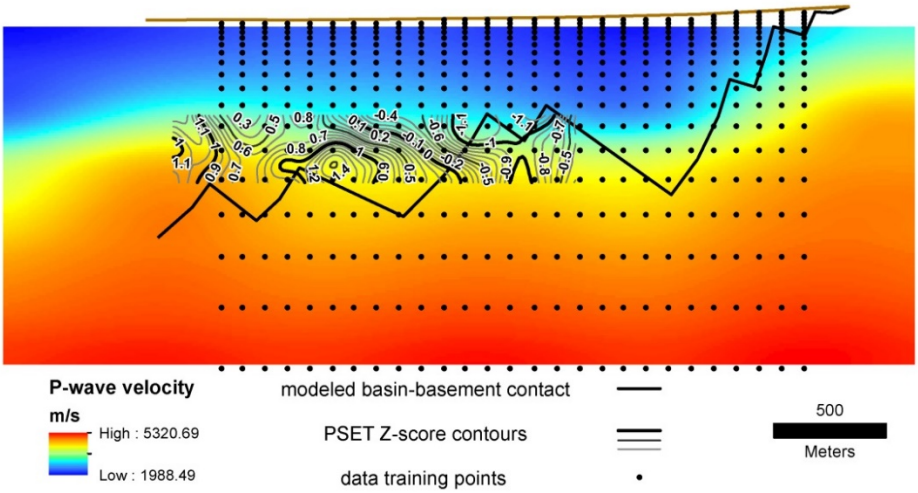

Figure 16: Cluster-analysis-refined P-wave velocity along the southernmost seismic line (#9) at San Emidio. Compare to original velocity determined from active seismic in Figure 4. Though smoothed, the data conform to the modeled basin-basement contact and the general trend of resistivity gradients (Figure 13). PSET acoustic energy contours show high energy anomalies near the basin-basement contact and above faults interpreted to control the topography of the contact.

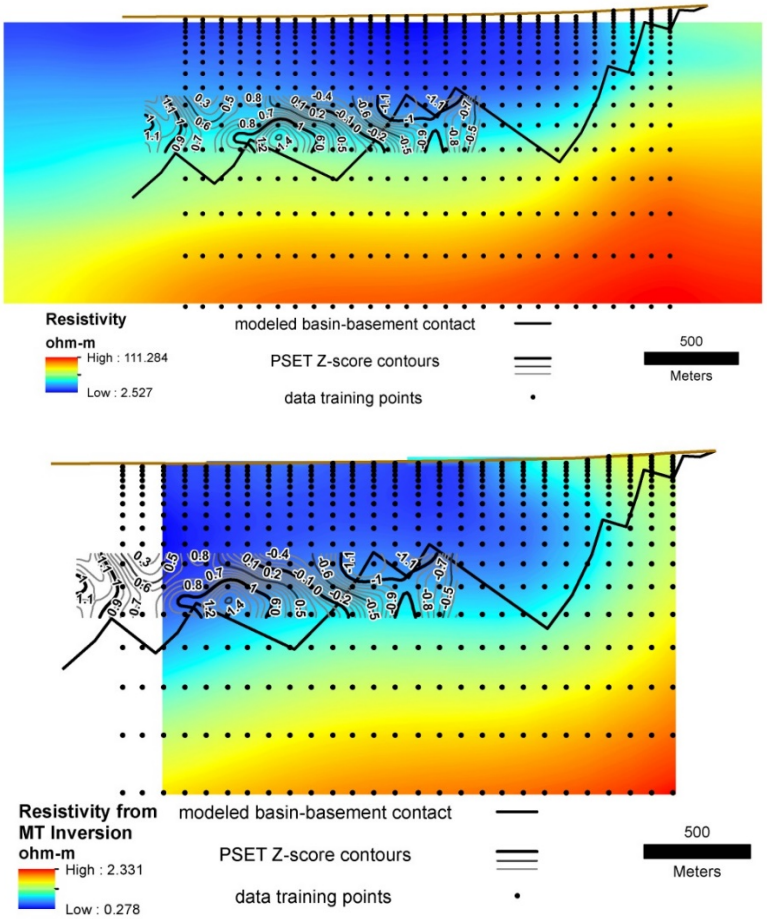

Figure 17: Cluster-analysis-refined resistivity and resistivity derived from MT inversion. Similar resistivity gradient patterns confirm the robustness of the cluster analysis.

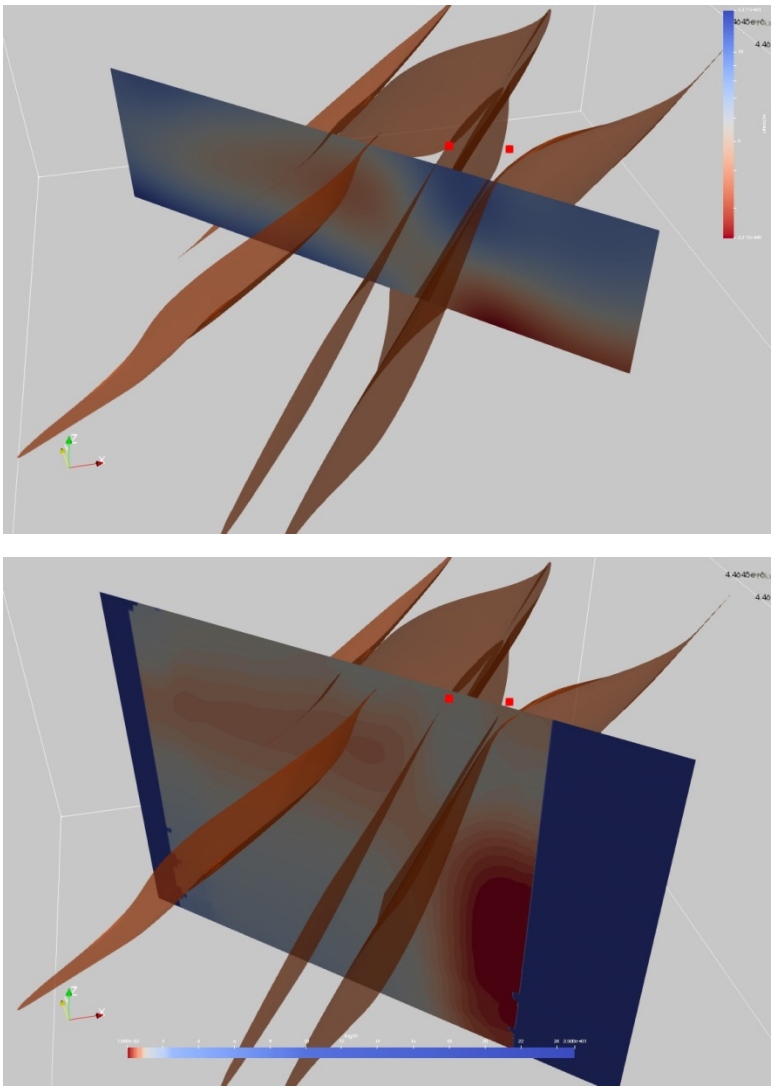

Figure 18: Oblique view looking down and to the north-northeast of neural-network-derived (top) and MT-derived (bottom) resistivity slices at Crescent Valley. Warm to cool colors correspond to low and high resistivity. Red squares are hot spring discharges.

6. San Emidio Permeability Mapping and Drill Targeting

Abundant datasets at San Emidio allow robust constraint and assessment of the PSET and MT datasets. Subsurface geology and location of permeable fractures are known from drilling; however, subsurface knowledge is incomplete. The project AOI is focused south of the currently exploited geothermal field (Figures 2, 6, and 10), and the western and southern extents of the southern resource area are unknown.

The drill targeting of Phase 2 will be based on integration of datasets into what is effectively a 3-D permeability map focused on locations most likely to allow drilling of successful geothermal wells. The main components of this map comprise total lost circulation zones (reservoir intersections) in wells, top of the reservoir/basement derived from 2-D gravity profile modeling, horizontal gradient magnitude from ground gravity and magnetics, faults interpreted from gravity

profile modeling and HGMs, measured and modeled subsurface temperature, PSET acoustic energy, and MT-derived resistivity.

On their own, both PSET acoustic energy and resistivity identify anomalous areas that coincide with structural targets (Figures 11 and 12). Acoustic energy anomalies mapped onto the top of the basement highlight areas where wells have intersected >320F reservoir; they occur within a broader low resistivity anomaly mapped on top of the basement. Viewed in 3-D, acoustic anomalies are somewhat diffuse, though they concentrate near the top of the basement in the vicinity of wells that intersect the reservoir (Figure 12). It is less clear how to use the 3-D resistivity volume for targeting without investigating its intersection with geologic surfaces. Low resistivity anomalies are more likely to be associated with clay-altered basin fill rather than conductive-brine-filled fracture and matrix porosity within relatively more resistant rock. The pattern of resistivity mapped on basement (Figure 12) extends >100m below the modeled basement elevation, providing confidence that the anomaly occurs beneath the generally clay-altered, low resistivity basin fill.

To further refine and quantify the targeting of high permeability, PSET semblance (sum at each xy location), magnetic HGM, gravity HGM, and resistivity of the top of basement are compared to well productivity (Figure 19). Gridded data were spatially queried to assign values at the location of each well lying within the AOI. Combination of variables were tested by summing the Z scores of the raw data values. The greatest contrast between permeable and tight wells is achieved using PSET semblance, magnetic HGM, and gravity HGM. Including the resistivity at the top of the basement did not improve differentiation of permeable from tight wells.

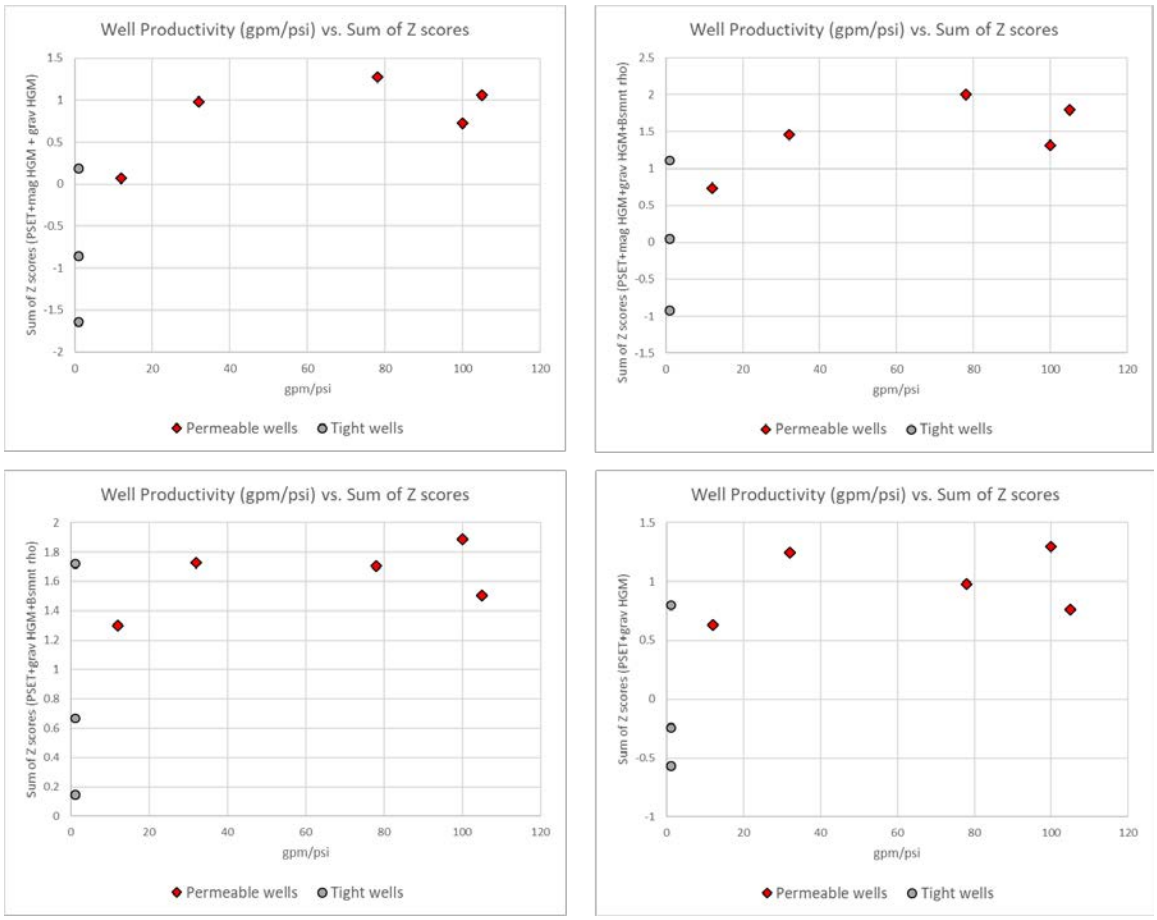

Figure 19. Well productivity compared to PSET semblance, top of basement/reservoir resistivity, and gravity and magnetics horizontal gradient magnitudes.

The anomalies defined by PSET semblance and gravity and magnetics HGMs highlight faults interpreted from the modeled top of the basement/reservoir. A significant, anomalous structure extends for more than 2 km from the northeast corner of the AOI to the southwest where it pinches out along the interpreted tip of a fault along which high productivity geothermal wells have been drilled (Figure 20). There is a possible cross fault that interrupts this anomalous structure north of wells 25-21 and 25A-21. Though not well constrained, this structure is suggested by multiple datasets and is likely NW-trending. The structure to the northwest of the drilled wells is also anomalous, and the hanging wall of this structure contains an anomaly that might be related to linkage between the two faults (Figure 20).

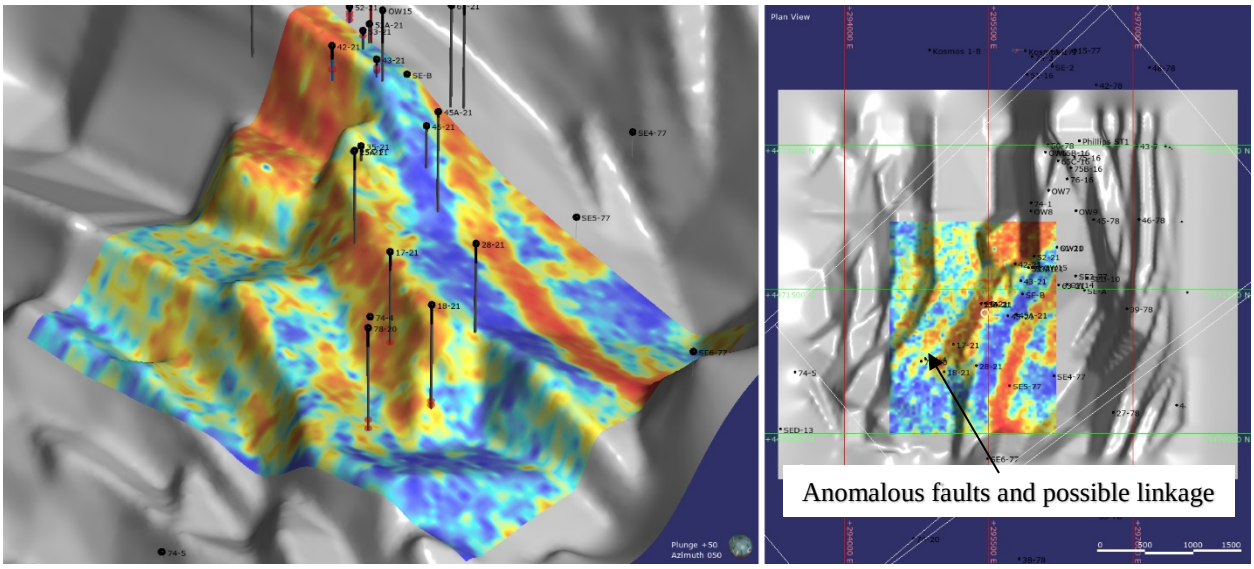

Figure 20. Sum of Z scores of PSET semblance and gravity and magnetics HGMs mapped onto the modeled top of basement/reservoir. High to low values are represented by warm to cool colors. The long NNE-trending anomaly to the southeast is interpreted to be a lithological feature since it is not associated with structure expressed in the topography of the basement.

PSET, resistivity and multi-variable anomalies have been partly tested with drilling of wells 17-21, 18-21, 25-21, 25A-21, and 78-20, all of which intersected high permeability fractures that produce >320F fluid. Tight and cooler wells have been drilled to the east of these wells, so the anomalous structure to the northwest would be considered the priority target away from already drilled high productivity wells. Additional targets could be located along strike and down dip of the structure already proven productive by drilling. The anomalies to the east cannot be completely ignored since shallow TG wells drilled by Chevron in the 1970s have high temperatures and gradients (Figure 21).

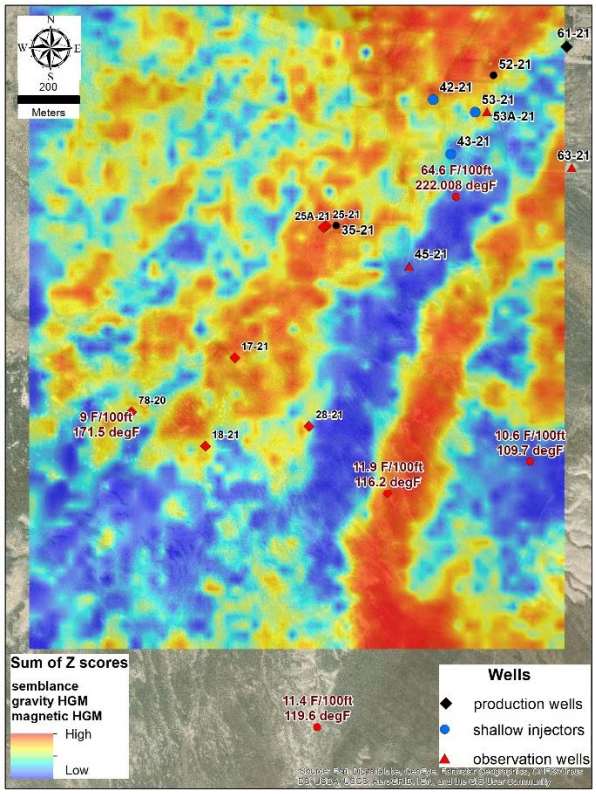

Figure 21. Shallow, high temperature and gradient TG wells overlie permeability anomalies defined by PSET semblance and gravity and magnetics HGMs east of the drilling defined, 320F+ resource. The main NNE-trending anomaly is not associated with any structure expressed in the topography of the top of the basement.

7. Crescent Valley Permeability Mapping and Drill Targeting

Using the same combination of datasets that best discriminate between tight and permeable wells at San Emidio, permeability anomalies were mapped at Crescent Valley (Figure 22). Gravity and magnetics HGMs emphasize the main range front fault and possible cross structures linking range-front-parallel faults. PSET semblance emphasizes faults located basin-ward of the main range front fault. The proposed target(s) are primarily guided by PSET, interpreted faults, and location basin-ward from hotsprings that discharge along the main range front fault.

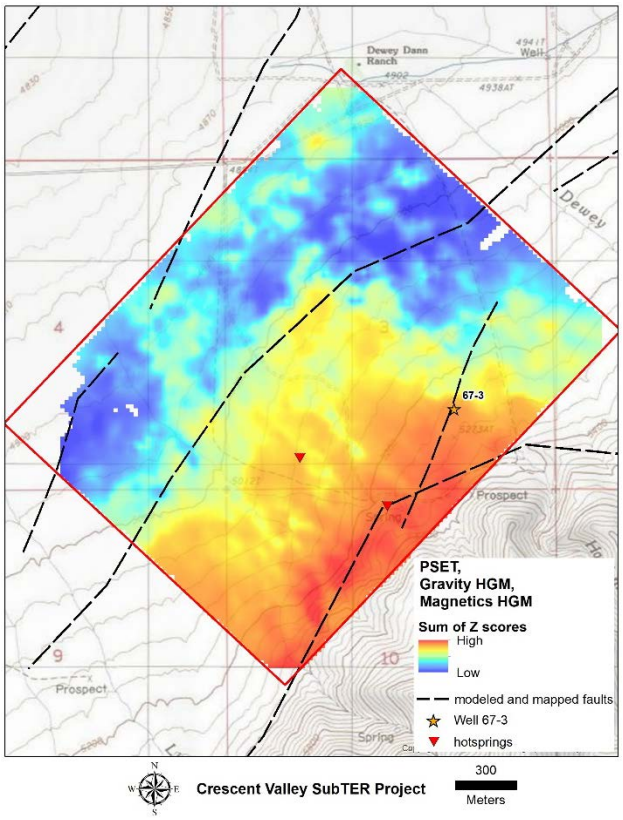

Figure 22. Permeability mapped with PSET semblance and gravity and magnetics HGMs. The main range front fault is highlighted; however, PSET semblance is more anomalous along the subparallel structure basin-ward of the range front (cf. Figure 13).

8. Conclusions

Analyses of passive seismic and MT data at San Emidio and Crescent Valley suggest that they are important components for generation of robust 3-D permeability maps for drill targeting. At both locations, resistivity contrasts map large-scale structure associated with range-front faults, and patterns of low resistivity correspond to basement rocks (sub-basin-fill) saturated with geothermal brine and/or affected by hydrothermal alteration. At San Emidio areas of high energy mapped with PSET correlate with areas of known permeability, and areas of low energy locally mark the currently understood boundaries of the newly discovered southern reservoir. The correlation between high energy and permeability is further strengthened with PSET data mapped onto faults and the top of reservoir rocks. At Crescent Valley the main range-front fault and subparallel faults in the hanging wall show high energy down dip and basin-ward from hot springs.

A seismic-MT cooperative inversion methodology developed with datasets from San Emidio allowed refinement of datasets using cluster analysis while honoring patterns of active-source-derived seismic velocities and MT-derived resistivity. Training of neural networks with these datasets has produced a model that can generate reasonable seismic velocity estimates based on the ability of the model to estimate velocity and resistivity values that preserve patterns observed in the original active-source derived seismic velocities and MT-derived resistivity datasets. Using

the cooperative inversion methodology, updated and refined velocity models were generated for processing of final PSET volumes at San Emidio and Crescent Valley.

PSET, resistivity, drilling, geology, gravity and magnetics datasets were integrated into a 3-D permeability map for drill targeting by comparing structural- and permeability-related datasets to the location of high productivity wells, and the xyz of total loss circulation zones, at San Emidio. A combination of PSET semblance (acoustic energy) and gravity and magnetics HGMs were determined to best discriminate between permeable and tight wells; anomalous areas defined by these variables coincide with the location of wells recently drilled into 320F+ resource. Using these permeability prediction maps, anomalous areas have been selected at San Emidio and Crescent Valley for drill testing in Phase 2.

Figure 23 shows proposed drill targets at San Emidio, both are located on BLM ground. The locations are within an area for which NEPA-related surveys and permitting activities are already in progress.

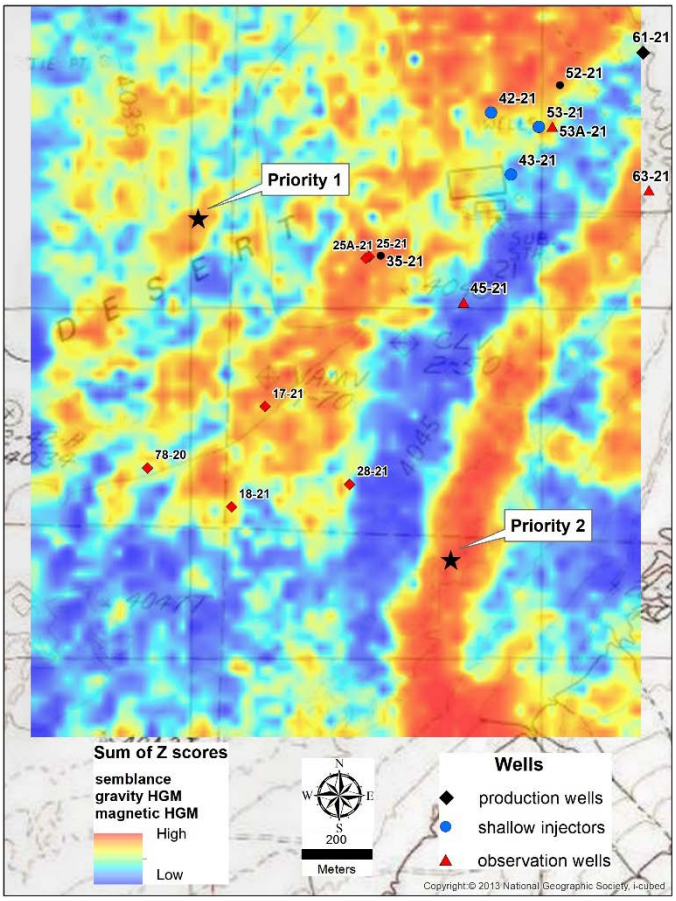

Figure 23. Proposed Phase 2 drill targets at San Emidio

Figure 24 shows the proposed drill target at Crescent Valley. It is located on private ground, so permitting and location adjustments can be made easily and quickly.

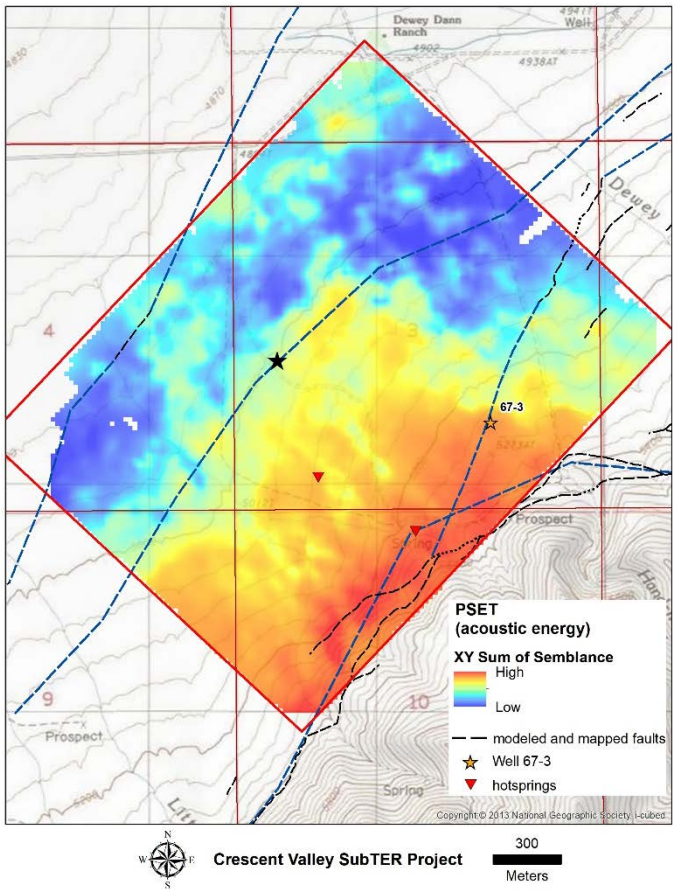

Figure 24. Proposed Phase 2 drill target at Crescent Valley

REFERENCES

Bennett, R.A., Wernicke, B.P., Niemi, N.A., Friedrich, A.M., and Davis, J.L., 2003, "Contemporary strain rates in the northern Basin and Range province from GPS data." *Tectonics*, v. 22, No. 2, p. 1-31.

Bezdek, J.C., 1973, "Cluster Validity with Fuzzy Sets." *Journal of Cybernetics*, 3(3):58-73.

Bezdek, J.C., 1974, "Numerical Taxonomy with Fuzzy Sets." *Journal of Mathematical Biology*, 1(1974):57-71.

Bezdek, J.C., Ehrlich, R., and Full, W., 1984, "FCM: The fuzzy c-means clustering algorithm." *Computers and Geosciences*, 10(2-3): 191-203.

Bonham, H.F., and Papke, K.G., 1969, "Geology and mineral deposits of Washoe and Storey Counties, Nevada." *Nevada Bureau of Mines and Geology Bulletin 70*, scale 1:250000, 140 p.

Drakos, P.S., 2007, "Tertiary stratigraphy and structure of the southern Lake Range, northwest Nevada: Assessment of kinematic links between strike-slip and normal faults in the northern Walker Lane [M.S. Thesis]." *University of Nevada*, Reno, 165 p.

Dunn, J.C., 1973, "A Fuzzy Relative of the ISODATA Process and Its Use in Detecting Compact Well-Separated Clusters." *Journal of Cybernetics*, 3(3): 32–57.

Eneva, M., Falorni, G., Teplow, W., Morgan, J., Rhodes, G., and Adams, D., 2011, "Surface deformation at the San Emidio Geothermal Field, Nevada, from satellite radar interferometry." *Geothermal Resources Council Transactions*, vol. 35, p. 1647-1654.

Faulds, J.E., Coolbaugh, M.F., Hinz, N.H., Cashman, P.H., and Kratt, C., Dering, G., Edwards, J., Mayhew, B., and McLachlan, H., 2011, "Assessment of favorable structural settings of geothermal systems in the Great Basin, western USA." *Geothermal Resources Council Transactions*, v. 35, p. 777-784.

Faulds, J.E., Hinz, N.H., Coolbaugh, M.F., dePolo, C.M., Siler, D.L., Shevenell, L.A., Hammond, W.C., Kreemer, C., and Queen, J.H., 2016, "Discovering Geothermal Systems in the Great Basin Region: An Integrated Geologic, Geochemical, and Geophysical Approach for Establishing Geothermal Play Fairways." *PROCEEDINGS, Forty-first Workshop on Geothermal Reservoir Engineering*, Stanford University, Stanford, California, February 22-24, 2016, 15 p.

Faust, L. Y., 1953, "A velocity function including lithologic variation." *Geophysics* 18(2): 271-288.

Gath, I. and A. B. Geva, 1989, "Unsupervised optimal fuzzy clustering." *IEEE Transactions on Pattern Analysis and Machine Intelligence*, 11(7):773-780.

Gustafson E. and Kessel, W., 2000, "Fuzzy clustering with a fuzzy covariance matrix." *In Proc. of IEEE CDC*, 1979, Hoppner,F., Klawonn, F., Kruse, R., and Runkler, T., Fuzzy Cluster Analysis, Methods for classification, data analysis and image recognition. Wiley.

Hacikoylu, P., Dvorkin, J., and Mavko, G., 2006, "Resistivity-velocity transforms revisited." *The Leading Edge*, v. 25:1006-1009.

Hammond, W.C. and Thatcher, W., 2005, "Northwest Basin and Range tectonic deformation observed with the Global Positioning System, 1999-2003." *Journal of Geophysical Research*, v.110, 12 p.

Hammond, W.C., Kreemer, C., and Blewitt, G., 2009, "Geodetic constraints on contemporary deformation in the northern Walker Lane: 3. Central Nevada seismic belt postseismic relaxation," in Oldow, J.S., and Cashman, P.H., eds., "Late Cenozoic Structure and Evolution of the Great Basin-Sierra Nevada Transition." *Geological Society of America Special Paper 447*, p. 33-54.

McConville, E.G., Faulds, J.E., Hinz, N.H., Ramelli, A.R., Coolbaugh, M.F., Shevenell, L., Siler, D.L., and Bourdeau-Hernikl, J., 2017, "A Play Fairway approach to geothermal exploration in Crescent Valley, Nevada." *Geothermal Resources Council Transactions*, v. 41, p. 1213-1221.

Rhodes, G.T., Faulds, J.E., and Teplow, W., 2010, "Structural controls of the San Emidio Desert Geothermal Field, northwestern Nevada.", *Geothermal Resources Council Transactions*, v. 34, p. 819-822.

Rhodes, G.T., Faulds, J.E., and Ramelli, A.R., 2011, "Preliminary Geologic Map of the Northern Lake Range, San Emidio Geothermal Area, Washoe County, Nevada." *Nevada Bureau of Mines and Geology Open-File 11-11*, 1:24,000 scale, 5p.

Teplow, W. and Warren, I., 2015, "Finding Large Aperture Fractures in Geothermal Resource Areas Using a Three-Component Long-Offset Surface Seismic Survey, PSInSAR and Kinematic Structural Analysis." *https://www.osti.gov/scitech/biblio/1213113-finding-large-aperture-fractures-geothermal-resource-areas-using-three-component-long-offset-surface-seismic-survey-psinsar-kinematic-structural-analysis*, 52p.

Ursin, B., and Carcione, J. M., 2007, "Seismic-Velocity/Electrical-Conductivity Relations." *EGM 2007 International Workshop Innovation in EM, Gravity and Mag Methods: a new Perspective for Exploration.*

Warren, I., Gasperikova, E., and Pullammanappallil, S., 2018, "Mapping Geothermal Permeability Using Passive Seismic Emission Tomography Constrained by Cooperative Inversion of Active Seismic and Electromagnetic Data." *PROCEEDINGS, Forty-third Workshop on Geothermal Reservoir Engineering*, Stanford University, Stanford, California, February 12-14, 2018, 14 p.

Werthmuller, D., Ziolkowski, A., and Wright, D., 2013, "Background resistivity model from seismic velocities." *Geophysics*, 78(4): E213-E223.

Xie, X. L. and Beni, G., 1991, "A validity measure for fuzzy clustering." *IEEE Transactions on Pattern Analysis and Machine Intelligence*, 13(8): 841-847.

Zadeh, L. A., 1965, "Fuzzy sets." *Information and Control*, 8(3): 338–353.